Renewable Energy 107 (2017) 531–541

Contents lists available at ScienceDirect

Renewable Energy

journal homepage: www.elsevier.com/locate/renene

Wind farm layout optimization using a Gaussian-based wake model☆

Leandro Parada [a, *], Carlos Herrera [b], Paulo Flores [a], Victor Parada [c]

[a] Department of Mechanical Engineering, University of Concepcion, Casilla 160 – C, Correo 3, Ciudad Universitaria, Concepción, Chile
[b] Department of Industrial Engineering, University of Concepcion, Casilla 160 – C, Correo 3, Ciudad Universitaria, Concepción, Chile
[c] Department of Computer Science, University of Santiago of Chile, Av. Ecuador 3659, Estación Central, Santiago, Chile

ARTICLE INFO

Article history:
Received 12 April 2016
Received in revised form
12 January 2017
Accepted 6 February 2017
Available online 11 February 2017

Keywords:
Wind farm
Wind turbine
Layout optimization
Micro-siting
Operations research
Genetic algorithms

ABSTRACT

The wind farm layout optimization problem has received considerable attention over the past two decades. The objective of this problem is to determine the wind farm layout that maximizes the annual energy generated. The majority of studies that have solved this problem simulated the velocity deficit using the Jensen wake model. However, this model is not in agreement with field measurements and computational fluid dynamics simulations. In this study, an approach to solve the wind farm layout optimization problem based on a Gaussian wake model is proposed. The Gaussian wake model uses an exponential function to evaluate the velocity deficit, in contrast to the Jensen wake model that assumes a uniform velocity profile inside the wake. The proposed approach minimizes the annual cost of energy of a wind farm using a genetic algorithm. The application of the proposed approach yields higher annual generation and a lower computational time for all wind scenarios under study. Under a more complex wind scenario, the improvement was relatively small. This suggests that the use of a more robust wake model in the WFLO problem, does not lead to greater efficiency in real wind cases.

1. Introduction

The worldwide installed capacity of wind energy could be greater than 800 GW by the year 2020 if the trend continues. The World Wind Energy Association (WWEA) has reported that during the year 2015, more than 60 GW of capacity was installed, reaching an overall installed capacity of 434 GW worldwide [1]. Over the past decade, 38 GW of capacity on average has been installed annually worldwide. The general trend in wind energy use can primarily be attributed to the constant increase in the price of fossil fuels and the increasing social awareness of the impacts of greenhouse gas emissions on climate change [2]. The rapidly growing wind energy market has led to new challenges. For instance, a substantial portion of the onshore sites with the best wind resources are already being exploited; therefore, wind farm operators and designers are looking for new methods to make profits. As an example, advanced control methods such as model predictive control can effectively maintain constant power output while reducing mechanical loads on wind turbines, and therefore, reduce overall wind farm costs [3,4]. At the wind farm design stage, one of the most promising topics that has received considerable attention over the past two decades is wind farm layout optimization. Wind farm layout optimization leads to higher power efficiency, and therefore, higher energy generation per unit area.

The wind farm layout optimization (WFLO) problem, also known as the optimal wind turbine micro-siting problem, is a highly complex optimization problem that was first presented by Mosetti et al. [5]. The objective of this problem is to maximize energy production by locating wind turbines in such a way that the wake interference between them is minimized. The WFLO problem is a highly complex optimization problem that, even for a low number of turbines ($N_t < 30$), can have more than 10^{44} potential solutions. In addition, it is a mixed integer problem (has integer and continuous variables), is highly non-convex (has many optimal solutions) and cannot be represented in analytical form [6,7]. Therefore, this problem cannot be solved using traditional optimization methods, such as calculus-based methods. Most authors have decided to approach this problem using meta-heuristics, which are a family of optimization techniques that provide acceptable solutions to complex problems in a reasonable computational time. Genetic algorithms are the most commonly used meta-heuristicts for approaching this problem because of their ability to avoid local optima in complex functions [8]. Other

☆ This document is a collaborative effort.
* Corresponding author.
E-mail address: lparada@udec.cl (L. Parada).

http://dx.doi.org/10.1016/j.renene.2017.02.017
0960-1481/

techniques to approach the WFLO include Particle swarm optimization [9–12], Ant colony optimization [13], Simulated annealing [14] and Artificial neural networks [15]. The high complexity of the problem is primarily due to the iterative evaluation of the velocity deficit caused by turbines in a wind farm, which must be calculated using an analytical wake model or by computational fluid dynamics (CFD).

The wake model proposed by Jensen [16,17], also known as the Park wake model, has been used in the vast majority of studies addressing the WFLO problem [7]. This model is very simple and it estimates the energy output accurately, as claimed by Katic et al. [17] [18]. However, field measurements of the velocity deficit in the wake of a wind turbine demonstrate that the velocity profile predicted by this model is unrealistic [19]. Due to the high complexity of the WFLO problem, it is not feasible to calculate the velocity deficit using computational fluid dynamics because the computational cost increases greatly, even for small problem instances. New analytic and semi-empirical wake models have been developed over the past decade. The velocity deficit described by these models is generally in agreement with computational fluid dynamics simulations and wind tunnel measurements [20–23]. These studies have demonstrated that the velocity profile in the wake of a wind turbine can be represented by a Gaussian curve [20,24]. In particular, Bastankhah and Porté-Agel [23] proposed a simple wake model that is based on a Gaussian curve and that only requires the specification of one parameter, the wake expansion factor k^*. This model has not been extended to the case of a wind farm with multiple wind turbines and has not yet been applied to predict the velocity deficit in the WFLO problem. In this study, the Gaussian-based wake model (GWM) proposed by Bastankhah and Porté-Agel [23] is extended to predict the velocity deficit in an entire wind farm, and subsequently, a method based on this wake model is proposed to approach the WFLO problem. A more robust approach for the WFLO problem can be developed using the GWM to calculate the velocity deficit. The proposed method uses a genetic algorithm to determine the individual positions of the turbines within a wind farm to minimize the annual cost of energy.

2. Gaussian-based wake model

Multiple studies have been conducted on the wake effect and turbulence caused by wind turbines. The studies that focused on modeling the wake of wind turbines can be classified into two classes: analytical models generally derived from empirical correlations and computational fluid dynamics-based models [7]. The second class includes methods based on large eddy simulation (LES) and Reynolds-averaged Navier-Stokes (RANS). These methods require considerable computational resources, making it practically infeasible to apply such methods within an iterative process, such as the wind farm layout design.

Analytical wake models are suitable for the WFLO problem because their computational cost is low and because it is easy to embed them within an optimization algorithm. The two most commonly used analytical models in WFLO studies are the model proposed by Jensen and the model proposed by Frandsen [5,25–28]. These models have been classified as top-hat models because they represent the velocity deficit in the radial direction by a discrete function. In fact, the velocity deficit some distance from the turbine rotor is approximately asymmetric [21,29] and resembles a Gaussian curve in the radial direction.

In this study, a wake model based on a Gaussian curve is used to predict the velocity deficit caused by wind turbines. This model was proposed by Bastankhah and Porté-Agel [23] and is based on the law of mass conservation and the law of momentum conservation. The GWM is based on the following equation for calculating the normalized velocity deficit:

$$\frac{\Delta u}{u_0} = C(x) f\left(\frac{r}{\delta(x)}\right), \tag{1}$$

where $C(x)$ represents the maximum normalized velocity deficit at a given downstream distance x. r is the radial distance measured from the center of the wind turbine, and $\delta(x)$ is the characteristic wake width at a given distance x. It is assumed that this characteristic wake width has a Gaussian shape, as shown in Fig. 1.

$$\frac{\Delta u}{u_0} = C(x)\exp\left(\frac{-r^2}{2\sigma^2}\right), \tag{2}$$

where σ is the standard deviation of the Gaussian-shaped velocity deficit at a given distance behind the turbine rotor. $C(x)$ is obtained by solving the equation of mass conservation and energy conservation, according to equation (3), where C_t is the thrust coefficient and d_0 is the rotor diameter:

$$C(x) = 1 - \sqrt{1 - \frac{C_t}{8(\sigma/d_0)^2}}. \tag{3}$$

Assuming a linear expansion of the wake region, as in Jensen's model, σ/d_0 can be obtained from the following equation:

$$\sigma/d_0 = k^*\frac{x}{d_0} + \varepsilon, \tag{4}$$

where $k^* = \delta\sigma/\delta x$ is the rate of growth of the wake and ε corresponds to the value of σ/d_0 when x tends to 0. Finally, introducing equations (3) and (4) into equation (2), the normalized velocity deficit is obtained through the following equation:

$$\frac{\Delta u}{u_0} = \left(1 - \sqrt{1 - \frac{C_t}{8(k^*x/d_0 + \varepsilon)^2}}\right) \times \exp\left(-\frac{1}{2(k^*x/d_0 + \varepsilon)^2}\left[\left(\frac{z - z_h}{d_0}\right)^2 + \left(\frac{y}{d_0}^2\right)\right]\right), \tag{5}$$

where z and y are the vertical and horizontal coordinates, respectively, and z_h is the hub height of the wind turbine. From equation (5), it follows that the calculation of the velocity deficit in the wake requires the determination of a single parameter (k^*). This parameter must be obtained from experimental data of the velocity profile, and therefore, varies with specific site parameters, such as the surface roughness (z_0) and turbulence intensity (I_0). For further details of the mathematical derivation of the model, refer to [23].

2.1. Comparison with Jensen's wake model

The GWM is simple, and it is in acceptable agreement with the LES simulations and wind tunnel measurements [23]. Bastankhah and Porté-Agel performed a comparison between the GWM wake model and two top-hat models (Jensen's [16] and Frandsen's [30]) in five case studies that involved miniature and real-scale wind turbines. In all cases, the velocity deficit calculated using the GWM was in acceptable agreement with LES simulations and wind tunnel measurements. In contrast, the top-hat models generally over predicted the velocity deficit in the center of the wake and under predicted the velocity deficit close to the edge of the wake.

Unlike Jensen's model [16], the GWM represents the velocity deficit with a continuous function in the radial direction. In Fig. 2, a comparison of the normalized velocity deficit calculated with both

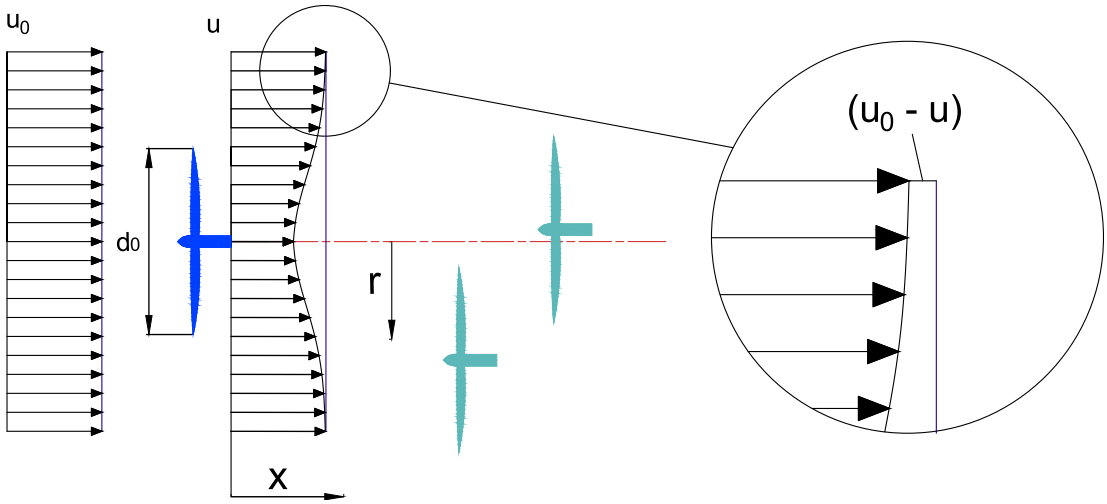

Fig. 1. Velocity profile of the wind behind a wind turbine calculated by the GWM.

models in the radial and streamwise directions is presented. For such simulations, a turbine with the following specifications is used: $D = 80m$, $z_h = 70m$, $z_0 = 0.5m$ and $C_t = 0.8$. The normalized radial distance is presented in the y-axis, and the normalized downstream distance is presented in the x-axis. Both models are valid for calculating the velocity deficit at a downstream distance greater than 3D from the turbine rotor (far wake region) [22,23,31].

Three major differences between the predicted wake development of both models can be observed in Fig. 2. First, it can be observed that in the radial direction, Jensen's model predicts a discrete distribution of the velocity deficit, whereas the GWM predicts a continuous distribution based on a Gaussian form. Second, it can be observed that the velocity deficit predicted by the GWM is high in comparison to that predicted by Jensen's model in the area closest to the turbine rotor ($3 \leq x/D \leq 5$). Finally, it can be observed that the velocity deficit predicted by the GWM recovers faster in the radial direction. This latter difference is best illustrated in Fig. 3. This figure presents a comparison of the velocity deficit predicted at 5D, 10D and 15D downstream of a turbine rotor. The characteristic top-hat shape of Jensen's model can be observed in this figure. In the three cases, as the radial distance increases from the center of the wake, the velocity deficit predicted by both models differs greatly.

2.2. Wake interference of multiple wind turbines

The effect of multiple wakes must be considered in a wind farm. Moreover, one should consider the effect of a turbine that is partially in the wake of another turbine [28]. The GWM is based on an exponential function for describing the velocity deficit; therefore, the radius of the wake expands indefinitely, as illustrated in Fig. 1. Consequently, all turbines located behind another (according to the wind direction) will be in the wake regardless of the distance between them. As a direct consequence, no turbine will be partially in the wake of another turbine.

Several methods for calculating the interference of multiple wakes exist in the literature. In this study, the method of Katic et al. [17] is used. This method is one of the most used methods in the literature and is based on the following assumption: *the sum of the kinetic energy deficit of a mixed wake is equal to the sum of the energy deficits for each wake at the calculated downwind position* [17]. Therefore, the velocity deficit δu_i of a wind turbine i due to the wake effect of N_t turbines may be defined as:

$$\delta u_i = \sqrt{\sum_{j=1}^{N_t} a_{ij} (\delta u_{ij})^2}, \tag{6}$$

where a_{ij} is a binary variable that assumes the value of 1 in the case that wind turbine i is in the wake of turbine j and 0 otherwise. Because the wake calculated with the GWM expands indefinitely, this variable assumes the value of 1 provided that turbine j is located in front of turbine i for a given wind direction θ^w. Therefore, the velocity deficit factor only depends on the location of each wind turbine on the wind farm and the direction of the wind.

3. Proposed approach for the WFLO problem

3.1. Mathematical optimization problem

In this section, the optimization problem used in the proposed approach is formulated. The WFLO problem is a mixed integer problem, is highly combinatorial, non-convex and cannot be represented in analytical form [6,7].

In the proposed approach, the variables of the optimization problem are the locations of each turbine on the wind farm. The proposed approach considers N_t turbines located on a flat terrain. The coordinates of every turbine on the wind farm are represented by a single vector X, as in (7), and it is assumed that all turbines on the wind farm are equal and have the same power curve.

$$X = \left[x_1\ y_1\ x_2\ y_2\ x_3\ y_3\ \ldots\ x_{N_t}\ y_{N_t}\right] \tag{7}$$

3.2. Wind turbine potential locations

Two wind farm grid densities are used in this study. The first is a discrete grid of 100 potential locations, as in Grady et al. [25]. The second is a finer grid with 400 potential locations based on the recommendations of recent studies [32,33]. Theoretically, this approach expands the solution space, which not only improves the results of optimization but also significantly increases the computational cost. In particular, Wang et al. [33] concluded that using a 20×20 grid produces better results and keeps the computational cost within an acceptable range. Therefore, the proposed approach considers a 10×10 grid and a 20×20 grid.

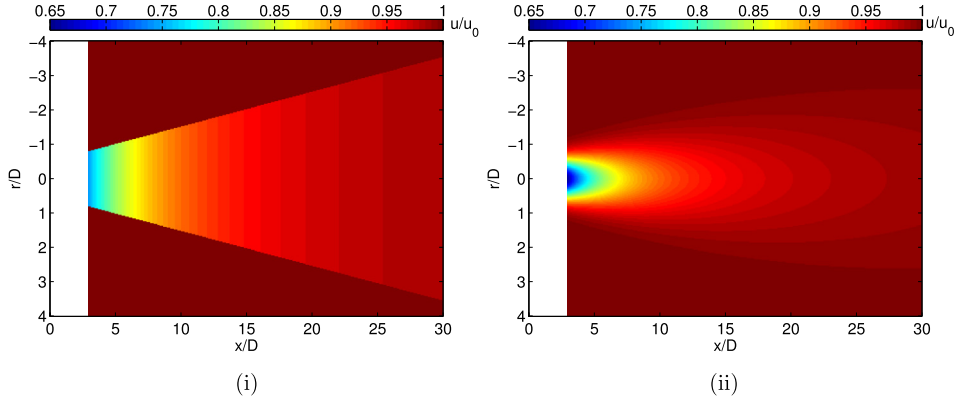

Fig. 2. Wake development of a single wind turbine calculated by (i) Jensen's model and (ii) GWM.

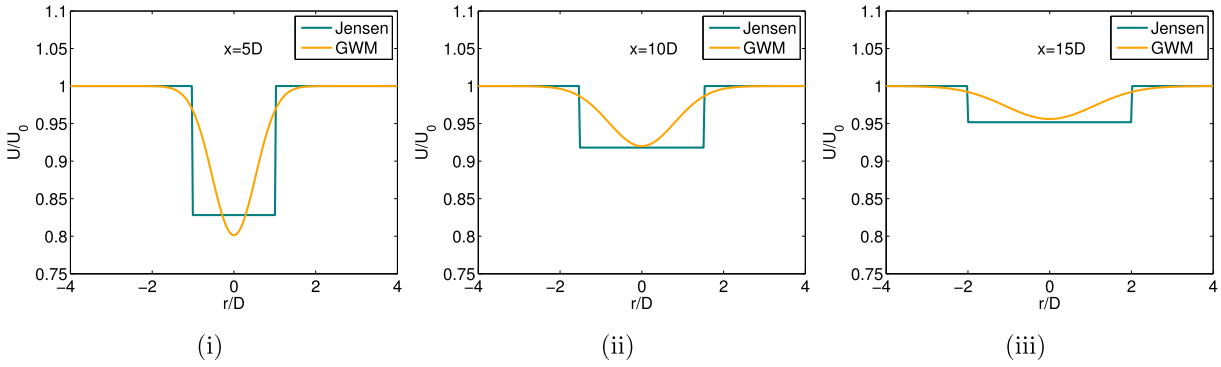

Fig. 3. Comparison of the velocity deficits predicted by both models at downstream distances of (i) 5D, (ii) 10D and (ii) 15D from the turbine rotor.

3.3. Objective function

The objective function to minimize is the cost of energy (CoE) given in (8), where $E(P)$ is the expected value of the power output from the wind farm.

$$CoE = \frac{C_{tot}}{E(P)}. \tag{8}$$

In the proposed approach, the number of hours a year that a wind farm generates electricity is considered to be constant; therefore, maximizing the power is equivalent to maximizing the annual energy generated (AEG).

The cost function used in this study is the same as that presented by Mosetti et al. [5] and is given in equation (9).

$$C_{tot} = N_t\left(\frac{2}{3} + \frac{1}{3}e^{-0.00174N_t^2}\right). \tag{9}$$

This function has been widely used in the literature, mainly because it is simple and represents the effect of economies of scale in wind farms. In this function, the annual dimensionless cost is directly related to the number of turbines N_t installed in the wind farm and consists of two terms: a constant term and a variable term that depends on an exponential function. The variable term decreases as the number of turbines increases, reaching a minimum when the wind farm has approximately 30 turbines.

The expected value of the power output from the wind farm for a fixed number of wind turbines can be represented by equation (10),

$$E(P) = \int_0^{360}\int_0^{\infty}\sum_{i=1}^{N_t} P_i(X;u,\theta^w)p(u,\theta^w)dud\theta^w, \tag{10}$$

where X is the vector containing the locations of all the turbines at the wind farm and $p(u,\theta^w)$ is the joint probability of wind speed u and wind direction θ^w. Integrating the wind speed between 0 and infinity is equivalent to integrating the wind speed between the cut-in speed and the cut-out speed [34]. The probability distributions of wind direction and speed can be discretized in N_θ and N_u bins, respectively. Therefore, the expected value of the power output from the wind farm can be approximated as the sum of the power produced by the turbines weighted by the probability of occurrence of the wind speed bin u_k and the wind direction bin θ_j, as presented in (11).

$$E(P) = \sum_{j=1}^{N_\theta}\sum_{k=1}^{N_u}\sum_{i=1}^{N_t} P_i\left(X;u_k,\theta_j^w\right)p\left(u_k,\theta_j^w\right). \tag{11}$$

To determine the velocity deficit factor of a turbine i under multiple wakes, it is necessary to know the locations of all turbines in the wind farm and the wind direction θ^w. We proposed the use of a passive transformation matrix to obtain the relative distances between turbines with respect to the wind direction. For example, consider the case of a turbine i that is in the wake of a turbine j when the wind blows in direction θ^w, as shown in Fig. 4. The coordinates of turbine i with respect to a north-west coordinates system with origin in turbine j are (x_i, y_i). By a passive transformation, the coordinates of turbine i with respect to a coordinate

system whose x-axis coincides with the wind direction and whose origin is on turbine j can be obtained. Therefore, the coordinates (x'_i, y'_i) of turbine i relative to the wind direction θ^w are obtained from the following equation:

$$(x'_i, y'_i) = (x_i, y_i) \cdot \begin{bmatrix} cos(\theta^w) & sin(\theta^w) \\ -sin(\theta^w) & cos(\theta^w) \end{bmatrix}. \quad (12)$$

After determining the relative distances between all turbines on the wind farm, the velocity deficit of each wind turbine must be calculated. Subsequently, the power of all the turbines is determined from the theoretical wind turbine power curve, as in Refs. [5,25]. Other more complex approaches to calculate the power include the wind turbine experimental power curve [6,28] and those used in predictive control strategies [4,35,36]. Once the power of the wind farm is determined, it is weighted by the probability of occurrence of wind speed and wind direction. Finally, the value of the cost of energy is calculated.

3.4. Constraints

A minimum distance of 5 rotor diameters between any two turbines within the wind farm is established:

$$d_{ij} = \sqrt{(x_i - x_j)^2 + \left(y_i - y_j\right)^2} > 5D, \quad \forall\ i,j = 1 \ldots N_t, i \neq j. \quad (13)$$

This minimum distance is set to reduce excessive loads on the turbines produced by high levels of turbulence in the near wake region [34]. In addition, the wake model used in this study is valid only for a downstream distance greater than or equal to $3D$ because, from this distance, the velocity deficit profile can be assumed to have a Gaussian shape [23]. Fig. 5 shows the infeasible region created by the proximity constraint. Turbines cannot be located in the red region surrounding each wind turbine.

3.5. A solution method based on a genetic algorithm

A genetic algorithm is an optimization procedure that is based on the competition of solutions. Each individual in the population represents a potential solution to a particular optimization problem. Initially, the population is generated randomly. An objective function associates the fitness of each individual with respect to the problem. Individuals reproduce to generate offspring using two variation operators: mutation and crossover. In each iteration, individuals are selected to be parents based on an acceptance criterion. This process is repeated until a stopping criterion is satisfied [8].

For the WFLO, each individual implicitly contains the coordinates of the locations of all the turbines of a wind farm. The fitness of each individual is the annual cost of energy of the wind farm, as shown in equation (8). In each iteration of the genetic algorithm, different configurations of wind farms are created by crossover, mutation and reproduction and are subsequently classified based on their fitness value. The best individuals survive and become parents of the next generation. The iterative process continues until the stopping criterion is met.

The genetic algorithm is implemented by OPTIMTOOL in MATLAB. The genetic algorithm corresponds to an extension of the LXPM algorithm called MI-LXPM that allows the use of integer variables [37]. This algorithm minimizes a penalty function rather than the fitness function. The penalty function allows infeasible solutions to be accepted, but it adds a term that depends on the violation of the constraints. Algorithm 1 shows the steps performed by the MI-LXPM genetic algorithm. First, a random population $g(t = 0)$ is created and evaluated. In each generation, tournament selection is applied over the previous generation $g(t-1)$ to obtain the set of individuals $g'(t)$. Subsequently, using a Laplace crossover strategy, a new set of individuals $g'(t)$ is obtained. Finally $g'(t)$ is produced using a Power mutation strategy. The stopping criterion used in this study is the number of generations N_{it} of the genetic algorithm. When the number of generations is reached, the best individual is returned.

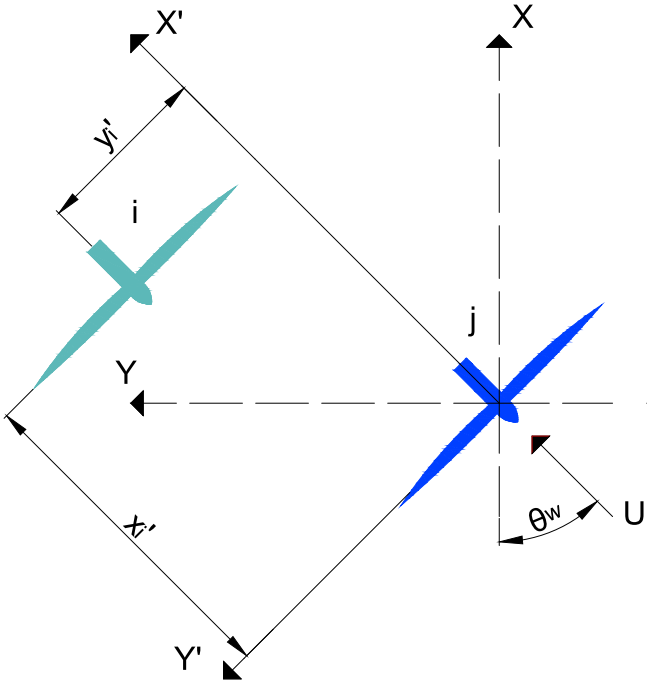

Fig. 4. Schematic representation of a wind turbine in the wake of another when the wind blows in direction θ^w.

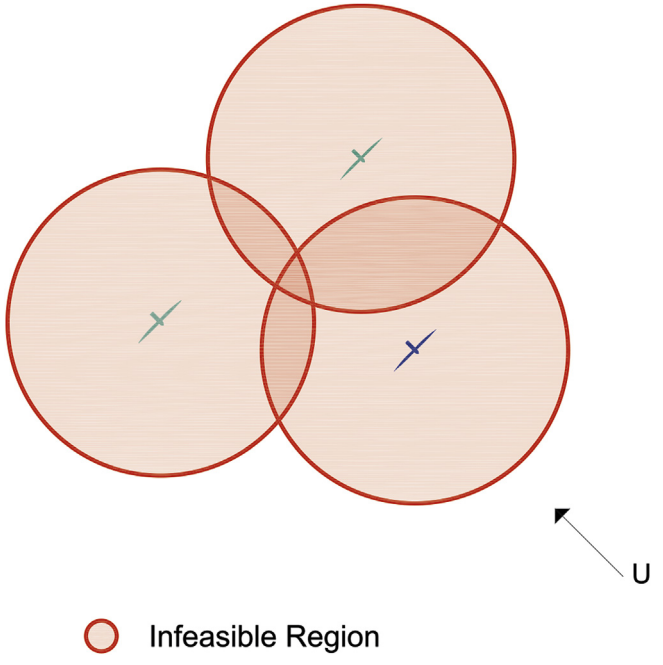

Fig. 5. Infeasible region created by the minimum distance between any two turbines in the wind farm (5D).

Algorithm 1 Genetic algorithm

Input: Population size ($popsize$) , Number of generations (N_{it}), Crossover probability (p_c), Mutation probability (p_m).

1: $t \longleftarrow 0$
2: Initialize and evaluate random population $g(t = 0)$.
3: **while** $i \leq N_{it}$ **do**
4: $g(t)$=Selection($g(t-1)$) /*Tournament selection*/
5: $g'(t)$=Reproduction($g(t)$) /*Laplace Crossover*/
6: $g''(t)$=Mutation($g'(t)$) /*Power Mutation*/
7: Evaluate($g''(t)$)
8: $t = t + 1$
9: **end while**

Output: Best individual.

4. Results and discussion

4.1. Case under study

The proposed approach is compared with Grady et al. [25], which considers three instances originally proposed by Mosetti et al. [5]. Several WFLO studies have compared their results with these three instances because they are relatively easy to replicate. The parameters of the turbine and the terrain used are shown in Table 1. The wind turbine power curve used in Grady's study is represented by a single equation:

$$P = \frac{1}{2}\rho A \eta_0 u_0^3 = 0,3u_0^3. \tag{14}$$

Jensen's model was used in Grady's study to calculate the velocity deficit in the wind farm. To perform a fair comparison, the layouts obtained in Grady's study are also evaluated using the GWM. Due to the lack of data of the velocity profile for the wind turbine used in this case study, the value of k^* is assumed to be 0.055, the same calculated in case 2 of Batankhah et al.'s study [23], because both terrains have a similar surface roughness. The three instances studied are summarized below:

(a) Wind with constant speed and direction: the wind is simulated with a constant speed of 12 m/s and blowing north ($\theta^w = 0^\circ$).
(b) Wind with variable direction and constant speed: the wind rose is divided in 36 sectors, and each one has the same probability of occurrence. The wind speed is maintained constant at 12 m/s.
(c) Wind with variable direction and variable speed: wind speed depends on the direction and may be 8, 12 or 17 m/s according to the discrete probability distribution shown in Fig. 6. It is assumed that the angles of the probability distribution were measured anticlockwise and that 0 is equivalent to north direction, as in the study of [5]. In addition to the cost of energy, the power efficiency of wind farms is used to analyze the effect of the wake in power generation. The power efficiency of a wind farm containing N_t turbines can be expressed by the following equation [38]:

$$\eta = \frac{\sum_{i=1}^{N_t} P_i\left(X, u_k, \theta_j^w\right)}{N_t P^*(u_k)}, \tag{15}$$

where P^* is the power of each turbine without considering the wake effect.

To perform a direct comparison with Grady's study, the same number of turbines is used for each wind scenario (30, 39 and 39 turbines, respectively). Each case was optimized using two different grid densities: 10×10 and 20×20. For each case, 5 independent runs of the genetic algorithm were performed, and the number of generations was set to 500.

4.2. Case a: constant wind speed and wind direction

In Grady's study, only one column of the grid was optimized because the Jensen wake model only depends on the downstream distance. Unlike Jensen's model, the GWM is a function of the

Table 1
Parameters used in Grady's study [25].

Parameter	Value
Hub height [m]	60
Diameter [m]	40
Wind farm size [km^2]	4
Surface roughness [m]	0.3
Wind speed [m/s]	12
Minimum distance [m]	200
Thrust coefficient	0.88
Air density [kg/m^3]	1.225

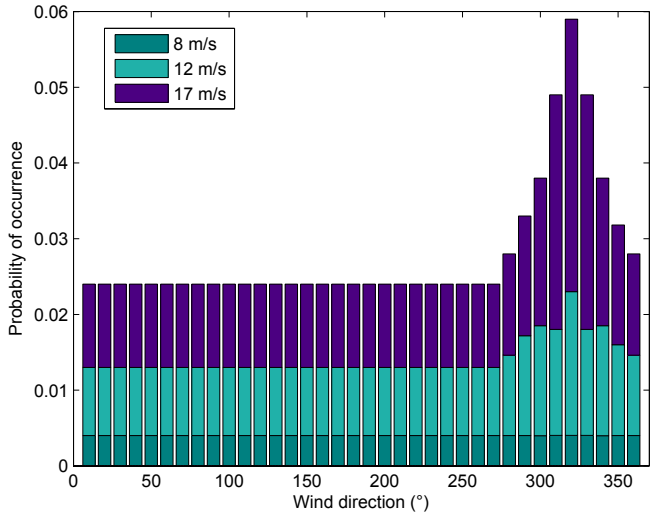

Fig. 6. Probability distribution of wind speed and direction for case c [5].

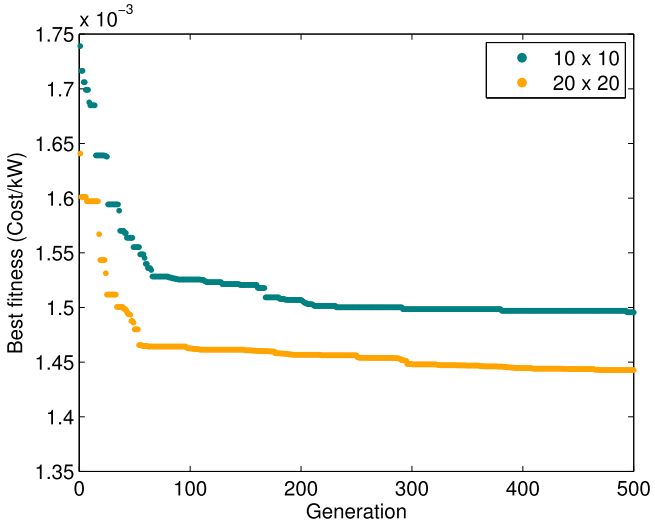

Fig. 7. Genetic algorithm convergence curves for case (a) using different grid densities.

downstream distance and the radial distance; therefore, all the layout must be optimized. Despite this fact, the layout optimized using a 10 × 10 grid is equal to that obtained by Grady. This is mainly because the size of each cell in the 10 × 10 grid (200[m]) is greater than the wake radius calculated using the GWM.

Under a constant wind condition, the proposed approach generates better solutions (greater power) when the terrain is subdivided in a finer grid. This phenomenon is illustrated in Fig. 7, in which both curves correspond to the best of the 5 genetic algorithm runs. The genetic algorithm performance improves considerably by increasing the number of potential locations, and therefore, a better layout is obtained.

The solution obtained using the proposed approach is characterized by an irregular layout of wind turbines when utilizing a finer grid (20 × 20). Fig. 8 presents a comparison between the layout optimized by Grady and those optimized using the proposed approach with the two different grid densities. As expected, the distance between the turbines is higher in the wind direction; however, in the case of the 20 × 20 grid, the solution is not a regular array as in the case of the 10 × 10 grid. The wake radius is smaller than the size of a cell in the 10 × 10 grid; therefore, in the 20 × 20 grid, the turbines are located closer in the radial direction. Despite the higher number of potential locations of the turbines in the 20 × 20 grid, the minimum distance between turbines is not violated. In the layout obtained using the proposed approach, no turbine experiences a velocity deficit higher than 2%. In contrast, in the layout proposed by Grady, all the turbines of the farthest row experience a velocity deficit of 3%.

Using the proposed approach with a 20 × 20 grid, a layout with 3.50% more power is obtained and with a computational cost that is 6 times lower. Table 2 summarizes the results obtained for case (a). The layouts obtained by Grady were also evaluated with the GWM, and the computational cost was measured as the number of generation times the number of individuals. The values in parentheses correspond to the results obtained directly by Grady using the Jensen model. The layout proposed by Grady evaluated with the GWM results in a better fitness value and therefore a better AEG. This result is primarily due to the faster recovery of the velocity deficit in the wake when using the GWM in this particular case. Consequently, the turbines in rows 6 and 10 experience less velocity deficit.

4.3. Case b: constant wind speed and variable wind direction

In this case, each angle has an equal probability of occurrence, which increases the complexity of the problem. Fig. 9 presents a comparison between the convergence curves of the best fitness obtained with a 10 × 10 grid and a 20 × 20 grid. This figure shows that the convergence curves of the proposed algorithm stabilized around the 300th generation. As shown in Fig. 9, a finer grid does not lead to a great improvement in fitness, in contrast to the result

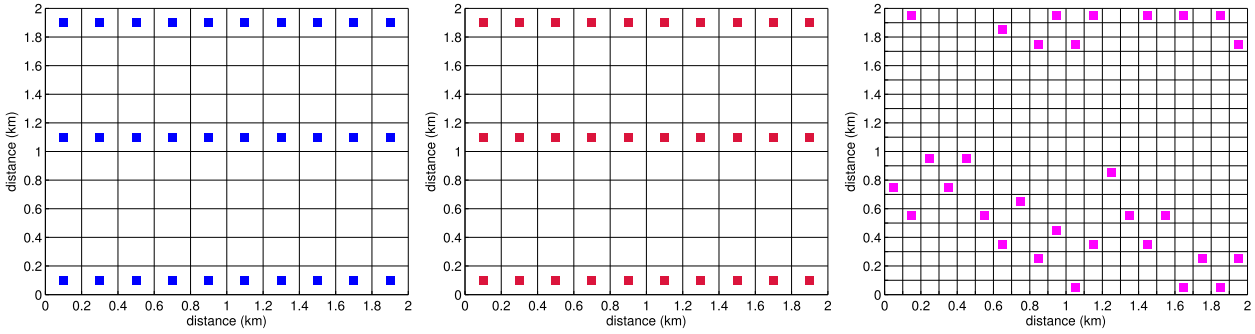

Fig. 8. Wind farm layouts for case (a) obtained by (i) Grady, (ii) proposed approach (10 × 10) and (iii) proposed approach (20 × 20).

Table 2
Comparison of results obtained for wind case (a).

Model	Grid	Fitness 10^{-3}	Power (MW)	Efficiency (%)	Computational cost (*gen indv*)
Grady	10 × 10	1.494 (1.543)	14.785 (14.310)	95.07 (92.02)	$1.8 \cdot 10^6$
Proposed	10 × 10	1.494	14.785	95.07	$3 \cdot 10^5$
Proposed	20 × 20	1.439	15.302	98.39	$3 \cdot 10^5$

Note: The values in parentheses correspond to the results obtained directly by Grady.

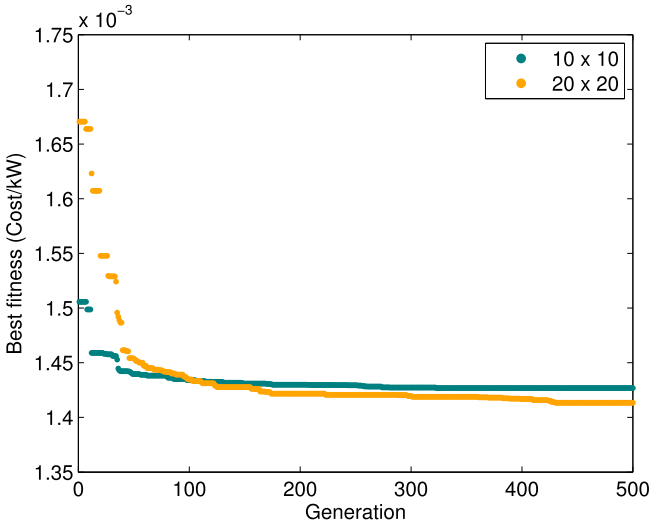

Fig. 9. Genetic algorithm convergence curves for case (b) using different grid densities.

obtained under a constant wind condition. In the 20 × 20 grid case, the proposed approach begins from a considerably worse initial solution; however, around the 130th generation, both curves intersect, and finally, a better solution is obtained with the densest grid. This phenomenon occurs because initially in the 20 × 20 case, solutions that violate the proximity constraint are generated and are therefore heavily penalized, unlike the 10 × 10 case.

The proposed approach generates solutions that have a tendency to locate the turbines in the outermost zone of the grid when considering a variable wind scenario. Fig. 10 presents a comparison between the layout optimized in Grady's study and those optimized using the proposed approach with the two grid densities. As shown in Fig. 10, in all three cases, the obtained wind farm layouts are irregular; however, in the layout obtained by Grady, the majority of the turbines are located in the central area of the grid. This result is in contrast to the layouts designed by the proposed approach, in which the majority of the turbines are located in the outermost zone of the grid.

A more efficient wind farm was obtained by the proposed approach for both grid sizes in a computational time that was 6 times lower. Table 3 presents a comparison of the results obtained for case (b). The layout optimized by Grady evaluated with the GWM results in an improvement of the fitness value; however, it is evident that this layout does not correspond to the optimum layout. In the case of a 10 × 10 grid, a 1.35% improvement in the efficiency was obtained, whereas in the case of a 20 × 20 grid, a 2.28% improvement was obtained. Part of the efficiency improvement is due to the turbines located in the outermost rows and columns of the layout. In the layout shown in Fig. 10 (iii), approximately 62% of the turbines are in the outermost zone of the terrain, in contrast to the layout optimized by Grady, in which only 51% of the turbines are located in this zone. One possible explanation for this phenomenon is that the velocity deficit recovers slightly faster in the GWM; thus, the turbines located in the central zone of the terrain are less influenced by the turbines located in the outer zone. Another important cause of the lower

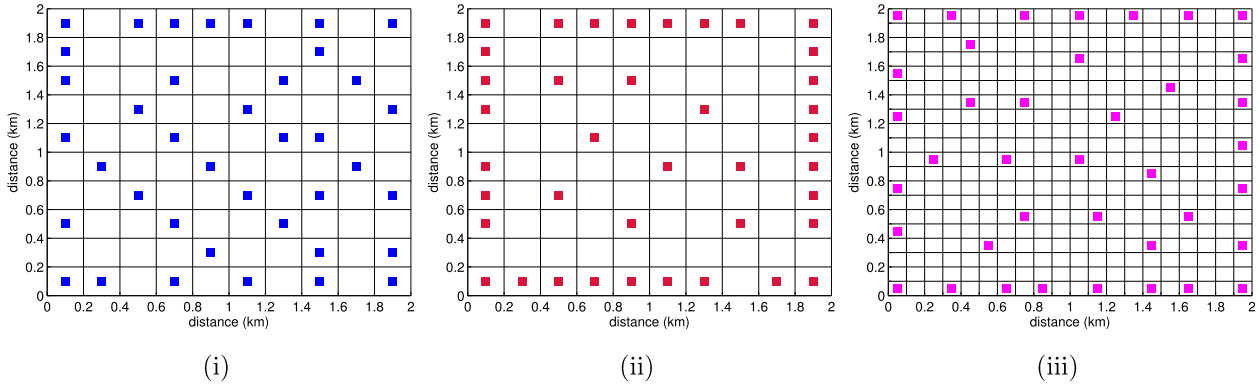

Fig. 10. Wind farm layouts for case (b) obtained by (i) Grady, (ii) proposed approach (10 × 10) and (iii) proposed approach (20 × 20).

Table 3
Comparison of results obtained for wind case (b).

Model	Grid	Fitness 10^{-3}	Power (MW)	Efficiency (%)	Computational cost (*gen indv*)
Grady	10 × 10	1.448 (1.567)	18.590 (17.220)	91.95 (85.174)	$1.8 \cdot 10^6$
Proposed	10 × 10	1.427	18.866	93.31	$3 \cdot 10^5$
Proposed	20 × 20	1.413	19.052	94.23	$3 \cdot 10^5$

Note: The values in parentheses correspond to the results obtained directly by Grady.

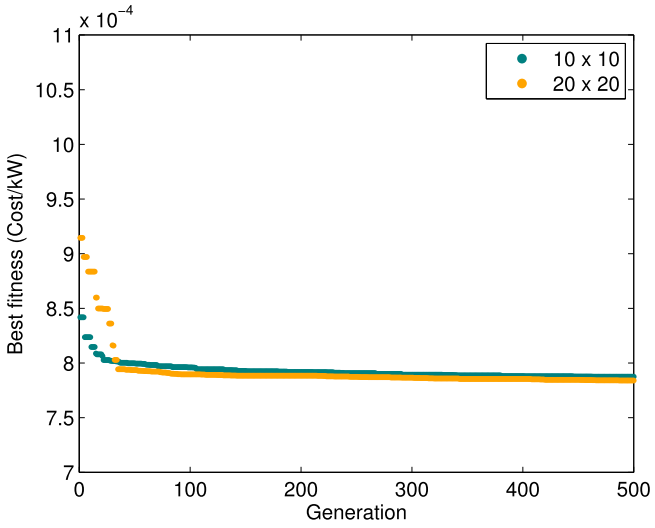

Fig. 11. Genetic algorithm convergence curves for case (c) using different grid densities.

efficiency of Grady's layout is the location of turbines in the center zone that are less than 8*D* apart. The Jensen model underpredicts the maximum velocity deficit, particularly for small distances ($x/d_0 \leq 8$) [23], leading to relatively high wake losses when evaluated with the GWM.

4.4. Case c: variable wind speed and wind direction

In this case, the speeds of 12 m/s and 17 m/s are predominant, particularly between the angles 280° and 360° (measured anti-clockwise) (see Fig. 6). Fig. 11 presents a comparison between the layout optimized in the study of Grady and those optimized using the proposed approach with the two grid densities. The first notable result in Fig. 11 is the low fitness value compared to the two previous cases. This result is primarily due to the high probability of occurrence of a wind speed of 17 m/s for all directions. The power curve used by Grady is proportional to u^3; therefore, a higher speed causes a cubic increase in power.

Fig. 12 presents the comparison between the layouts. As in the previous case, the layouts optimized by the proposed approach are scattered and irregular. Turbines are located primarily in the outermost zone of the wind farm, particularly on the prevailing wind directions ($270^\circ - 350^\circ$).

The higher complexity in the wind scenario causes less improvement in efficiency and power than in the previous cases. Table 4 presents a comparison of the main results obtained for case (c). As in case (b), the difference between the layouts optimized with different grid densities is small. The wind farm efficiency improved only 0.37% and 0.82% for both grid densities, respectively. In contrast to the other two cases, the improvement with respect to the layout optimized by Grady is considerably smaller.

5. Conclusion

An approach for designing highly efficient wind farm layouts was presented. The model used to calculate the velocity deficit between the wind turbines is a Gaussian-based wake model [23]. The velocity deficit predicted by the GWM is generally in acceptable agreement with LES simulations and wind tunnel measurements [23]. A genetic algorithm was adopted to approach the optimization problem. The proposed approach minimizes the annual cost of energy of a wind farm by placing the wind turbines in such a way that the wake loss is the minimum.

The proposed approach was compared to the results obtained by Grady et al. [25] on three wind cases; (a) wind with constant speed and direction, (b) wind with variable direction and constant speed and (c) wind with variable direction and variable speed. For the three wind cases, better results were obtained using the proposed approach in a lower computational time. For a more complex wind scenario (case (c)), the improvement was considerably lower than for cases (a) and (b). This suggest that the use of a more complex wake model in the WFLO problem, such as the GWM, does not lead to greater efficiency for real wind cases. Considering the inherent

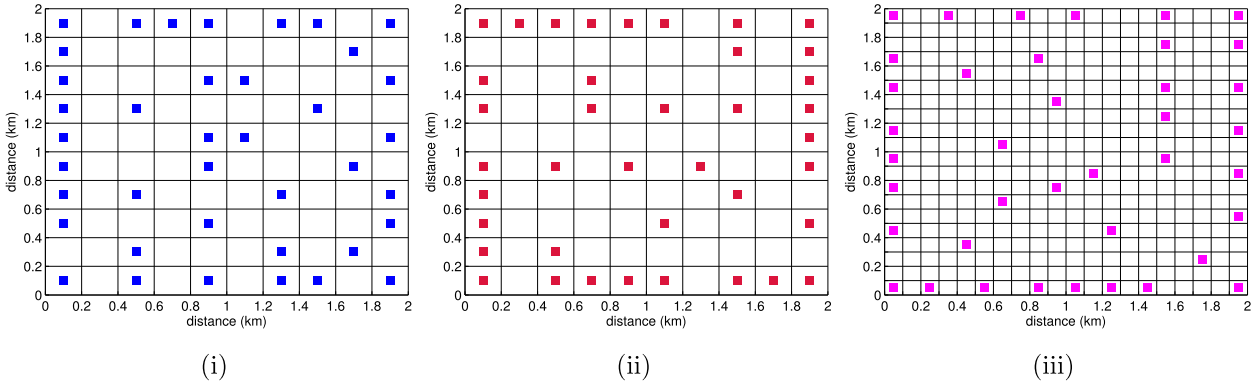

Fig. 12. Wind farm layouts for case (c) obtained by (i) Grady, (ii) proposed approach (10 × 10) and (iii) proposed approach (20 × 20).

Table 4
Comparison of results obtained for wind case (c).

Model	Grid	Fitness 10^{-4}	Power (MW)	Efficiency (%)	Computational cost (*gen indv*)
Grady	10 × 10	7.909 (8.031)	34.040 (32.038)	93.25 (86.62)	$6{\cdot}10^5$
Proposed	10 × 10	7.875	34.173	93.62	$3{\cdot}10^5$
Proposed	20 × 20	7.840	34.338	94.07	$3{\cdot}0^5$

Note: The values in parentheses correspond to the results obtained directly by Grady.

high complexity of the WFLO problem, the reduction in the computational time justifies the use of the GWM. Moreover, the GWM predicts the velocity deficit with less uncertainty, and therefore, the proposed model is a more robust approach towards the WFLO. Nonetheless, factors not considered in this study, for example complex terrain or different site characteristics, should also be evaluated to reach an overall conclusion.

The use of a greater number of potential locations gives rise to more efficient wind farms under a constant wind scenario. However, under a variable wind scenario, the improvement is smaller. Although several authors [32,33,39] emphasize the use of a finer grid or a continuous search space for the WFLO problem, the results of this study show that the improvement is small under a more complex wind scenario (wind cases b and c).

Acknowledgment

This research was partially funded by ICM-FIC: P05-004-F and CONICYT: FB016.

References

[1] W. W. E. Association, The World Sets New Wind Installations Record: 63,7 GW New Capacity in 2015, Tech. rep, Feb. 2016, http://www.wwindea.org/the-world-sets-new-wind-installations-record-637-gw-new-capacity-in-2015/.
[2] J. Gonzalez, M. Burgos Payan, J. Riquelme-Santos, Optimization of wind farm turbine layout including decision making under risk, IEEE Syst. J. 6 (1) (2012) 94–102, http://dx.doi.org/10.1109/JSYST.2011.2163007.
[3] S. Bououden, M. Chadli, H.R. Karimi, Robust Predictive Control of a variable speed wind turbine using the LMI formalism, in: 2014 European Control Conference (ECC), 2014, pp. 820–825, http://dx.doi.org/10.1109/ECC.2014.6862277.
[4] S. Bououden, M. Chadli, S. Filali, A. El Hajjaji, Fuzzy model based multivariable predictive control of a variable speed wind turbine: LMI approach, Renew. Energy 37 (1) (2012) 434–439, http://dx.doi.org/10.1016/j.renene.2011.06.025. http://linkinghub.elsevier.com/retrieve/pii/S096014811100317X.
[5] G. Mosetti, C. Poloni, B. Diviacco, Optimization of wind turbine positioning in large windfarms by means of a genetic algorithm, J. Wind Eng. Ind. Aerodynam. 51 (1) (1994) 105–116, http://dx.doi.org/10.1016/0167-6105(94)90080-9. http://www.sciencedirect.com/science/article/pii/0167610594900809.
[6] J. Serrano González, M. Burgos Payán, J.M.R. Santos, F. González-Longatt, A review and recent developments in the optimal wind-turbine micro-siting problem, Renew. Sustain. Energy Rev. 30 (2014) 133–144, http://dx.doi.org/10.1016/j.rser.2013.09.027. http://linkinghub.elsevier.com/retrieve/pii/S1364032113006989.
[7] J. Herbert-Acero, O. Probst, P.-E. Réthoré, G. Larsen, K. Castillo-Villar, A review of methodological approaches for the design and optimization of wind farms, Energies 7 (11) (2014) 6930–7016, http://dx.doi.org/10.3390/en7116930. http://www.mdpi.com/1996-1073/7/11/6930/.
[8] E.-G. Talbi, Metaheuristics: from Design to Implementation, John Wiley & Sons, 2009.
[9] S. Pookpunt, W. Ongsakul, Optimal placement of wind turbines within wind farm using binary particle swarm optimization with time-varying acceleration coefficients, Renew. Energy 55 (2013) 266–276, http://dx.doi.org/10.1016/j.renene.2012.12.005. http://linkinghub.elsevier.com/retrieve/pii/S0960148112007604.
[10] C. Wan, J. Wang, G. Yang, X. Zhang, Optimal micro-siting of wind farms by particle swarm optimization, in: D. Hutchison, T. Kanade, J. Kittler, J.M. Kleinberg, F. Mattern, J.C. Mitchell, M. Naor, O. Nierstrasz, C. Pandu Rangan, B. Steffen, M. Sudan, D. Terzopoulos, D. Tygar, M.Y. Vardi, G. Weikum, Y. Tan, Y. Shi, K.C. Tan (Eds.), Advances in Swarm Intelligence, vol. 6145, Springer Berlin Heidelberg, Berlin, Heidelberg, 2010, pp. 198–205, http://dx.doi.org/10.1007/978-3-642-13495-1_25.
[11] C. Xu, J. Yang, C. Li, W.Z. Shen, Y. Zheng, D. Liu, A research on wind farm micro-sitting optimization in complex terrain, in: International Conference on Aerodynamics of Offshore Wind Energy Systems and Wakes (ICOWES 2013), 2013, pp. 669–679. http://orbit.dtu.dk/fedora/objects/orbit:125021/datastreams/file_44a90f17-7383-437e-b015-fc810d2d3175/content.
[12] S. Chowdhury, J. Zhang, A. Messac, L. Castillo, Optimizing the arrangement and the selection of turbines for wind farms subject to varying wind conditions, Renew. Energy 52 (2013) 273–282, http://dx.doi.org/10.1016/j.renene.2012.10.017. http://www.sciencedirect.com/science/article/pii/S0960148112006544.
[13] Y. Eroğlu, S.U. Seçkiner, Design of wind farm layout using ant colony algorithm, Renew. Energy 44 (2012) 53–62, http://dx.doi.org/10.1016/j.renene.2011.12.013. http://www.sciencedirect.com/science/article/pii/S096014811100694X.
[14] R.A. Rivas, J. Clausen, K.S. Hansen, L.E. Jensen, Solving the turbine positioning problem for large offshore wind farms by simulated annealing, Wind Eng. 33 (3) (2009) 287–297.
[15] L. Ekonomou, S. Lazarou, G.E. Chatzarakis, V. Vita, Estimation of wind turbines optimal number and produced power in a wind farm using an artificial neural network model, Simul. Model. Pract. Theory 21 (1) (2012) 21–25, http://dx.doi.org/10.1016/j.simpat.2011.09.009. http://www.sciencedirect.com/science/article/pii/S1569190X11001626.
[16] N. Jensen, A Note on Wind Generator Interaction, Tech. Rep. 87-550-0971-9, 1983.
[17] I. Katic, J. Højstrup, N. Jensen, A simple model for cluster efficiency, in: EWEC'86. Proceedings, vol. 1, 1987, pp. 407–410.
[18] M. Magnusson, A.S. Smedman, Air flow behind wind turbines, J. Wind Eng. Ind. Aerodynam. 80 (1–2) (1999) 169–189, http://dx.doi.org/10.1016/S0167-6105(98)00126-3. http://www.sciencedirect.com/science/article/pii/S0167610598001263.
[19] L.J. Vermeer, J.N. Sørensen, A. Crespo, Wind turbine wake aerodynamics, Prog. Aerosp. Sci. 39 (6–7) (2003) 467–510, http://dx.doi.org/10.1016/S0376-0421(03)00078-2. http://www.sciencedirect.com/science/article/pii/S037604210300078 2.
[20] J.F. Ainslie, Calculating the flowfield in the wake of wind turbines, J. Wind Eng. Ind. Aerodynam. 27 (1–3) (1988) 213–224, http://dx.doi.org/10.1016/0167-6105(88)90037-2. http://www.sciencedirect.com/science/article/pii/0167610588900372.
[21] J. Bartl, F. Pierella, L. Sætrana, Wake measurements behind an array of two model wind turbines, Energy Proc. 24 (2012) 305–312, http://dx.doi.org/10.1016/j.egypro.2012.06.113. http://www.sciencedirect.com/science/article/pii/S1876610212011538.
[22] L. Tian, W. Zhu, W. Shen, N. Zhao, Z. Shen, Development and validation of a new two-dimensional wake model for wind turbine wakes, J. Wind Eng. Ind. Aerodynam. 137 (2015) 90–99, http://dx.doi.org/10.1016/j.jweia.2014.12.001. http://linkinghub.elsevier.com/retrieve/pii/S0167610514002505.
[23] M. Bastankhah, F. Porté-Agel, A new analytical model for wind-turbine wakes, Renew. Energy 70 (2014) 116–123, http://dx.doi.org/10.1016/j.renene.2014.01.002. http://www.sciencedirect.com/science/article/pii/S0960148114000317.
[24] Y.-T. Wu, F. Porté-Agel, Atmospheric turbulence effects on wind-turbine wakes: an LES study, Energies 5 (12) (2012) 5340–5362, http://dx.doi.org/10.3390/en5125340. http://www.mdpi.com/1996-1073/5/12/5340/.
[25] S. Grady, M. Hussaini, M. Abdullah, Placement of wind turbines using genetic algorithms, Renew. Energy 30 (2) (2005) 259–270, http://dx.doi.org/10.1016/j.renene.2004.05.007. http://linkinghub.elsevier.com/retrieve/pii/S0960148104001867.
[26] S. Şişbot, Z. Turgut, M. Tunç, N. Çamdal, Optimal positioning of wind turbines on Gökçeada using multi-objective genetic algorithm, Wind Energy 13 (4) (2010) 297–306, http://dx.doi.org/10.1002/we.339. http://onlinelibrary.wiley.com/doi/10.1002/we.339/abstract.
[27] Y. Chen, H. Li, K. Jin, Q. Song, Wind farm layout optimization using genetic algorithm with different hub height wind turbines, Energy Convers. Manag. 70 (2013) 56–65, http://dx.doi.org/10.1016/j.enconman.2013.02.007. http://linkinghub.elsevier.com/retrieve/pii/S0196890413000873.
[28] J.S. González, A.G. Gonzalez Rodriguez, J.C. Mora, J.R. Santos, M.B. Payan, Optimization of wind farm turbines layout using an evolutive algorithm, Renew. Energy 35 (8) (2010) 1671–1681, http://dx.doi.org/10.1016/j.renene.2010.01.010. http://linkinghub.elsevier.com/retrieve/pii/S0960148110000145.
[29] L.P. Chamorro, F. Porté-Agel, A wind-tunnel investigation of wind-turbine wakes: boundary-layer turbulence effects, Boundary-layer Meteorol. 132 (1) (2009) 129–149, http://dx.doi.org/10.1007/s10546-009-9380-8.
[30] S. Frandsen, R. Barthelmie, S. Pryor, O. Rathmann, S. Larsen, J. Højstrup, M. Thøgersen, Analytical modelling of wind speed deficit in large offshore wind farms, Wind Energy 9 (1–2) (2006) 39–53, http://dx.doi.org/10.1002/we.189. http://onlinelibrary.wiley.com/doi/10.1002/we.189/abstract.
[31] R.J. Barthelmie, L. Folkerts, G.C. Larsen, K. Rados, S.C. Pryor, S.T. Frandsen, B. Lange, G. Schepers, Comparison of wake model simulations with offshore wind turbine wake profiles measured by sodar, J. Atmos. Ocean. Technol. 23 (2006) 888, http://dx.doi.org/10.1175/JTECH1886.1. http://adsabs.harvard.edu/abs/2006JAtOT.23.888B.
[32] M. Samorani, The wind farm layout optimization problem, in: P.M. Pardalos, S. Rebennack, M.V.F. Pereira, N.A. Iliadis, V. Pappu (Eds.), Handbook of Wind Power Systems, Springer Berlin Heidelberg, Berlin, Heidelberg, 2013, pp. 21–38, http://dx.doi.org/10.1007/978-3-642-41080-2_2.
[33] L. Wang, A.C.C. Tan, Y. Gu, Comparative study on optimizing the wind farm layout using different design methods and cost models, J. Wind Eng. Ind. Aerodynam. 146 (2015) 1–10, http://dx.doi.org/10.1016/j.jweia.2015.07.009. http://www.sciencedirect.com/science/article/pii/S0167610515001725.
[34] A. Kusiak, Z. Song, Design of wind farm layout for maximum wind energy capture, Renew. Energy 35 (3) (2010) 685–694, http://dx.doi.org/10.1016/j.renene.2009.08.019. http://linkinghub.elsevier.com/retrieve/pii/S0960148109003796.
[35] N. Nanayakkara, M. Nakamura, H. Hatazaki, Predictive control of wind turbines in small power systems at high turbulent wind speeds, Control Eng. Pract. 5 (8) (1997) 1063–1069, http://dx.doi.org/10.1016/S0967-0661(97)00097-X. http://www.sciencedirect.com/science/article/pii/S096706619700097X.

[36] M. Jafarian, A. Ranjbar, Fuzzy modeling techniques and artificial neural networks to estimate annual energy output of a wind turbine, Renew. Energy 35 (9) (2010) 2008–2014, http://dx.doi.org/10.1016/j.renene.2010.02.001. http://linkinghub.elsevier.com/retrieve/pii/S0960148110000509.

[37] K. Deep, K.P. Singh, M.L. Kansal, C. Mohan, A real coded genetic algorithm for solving integer and mixed integer optimization problems, Appl. Math. Comput. 212 (2) (2009) 505–518, http://dx.doi.org/10.1016/j.amc.2009.02.044. http://www.sciencedirect.com/science/article/pii/S0096300309001830.

[38] J. Park, K.H. Law, Layout optimization for maximizing wind farm power production using sequential convex programming, Appl. Energy 151 (2015) 320–334, http://dx.doi.org/10.1016/j.apenergy.2015.03.139. http://linkinghub.elsevier.com/retrieve/pii/S0306261915004560.

[39] P. Mittal, K. Kulkarni, K. Mitra, A novel hybrid optimization methodology to optimize the total number and placement of wind turbines, Renew. Energy 86 (2016) 133–147, http://dx.doi.org/10.1016/j.renene.2015.07.100. http://www.sciencedirect.com/science/article/pii/S0960148115301956.